AJEMA GLOBAL RESEARCH NETWORK

AMERICAN Journal of Engineering, Mechanics and Architecture
Volume 4, Issue 02, 2026 ISSN (E): 2993-2637

Hybrid Composite Laminates using an AUXETIC Steel Core: A Numerical Investigation

Murtadha Saeed Mohammed, Mahmood S. Mahmood
Mechanical Engineering Department, University of Misan, Misan, Iraq

Abstract: The use of Fiber Metal Laminates (FMLs) provides a high-stiffness fibre-reinforced polymer (FRP) with ductile properties derived from metals; however, few studies have attempted to create hybrid FMLs that incorporate auxetic (negative Poisson's ratio) materials to enhance energy absorption characteristics. To investigate the mechanical behaviour of hybrid laminates composed of perforated steel metamaterials sandwiched between layers of Glass Fiber Reinforced Polymer (GFRP) and Carbon Fibers, a series of parametric studies using Finite Element Analysis (FEA) in SIMULIA Abaqus were conducted. This analysis focused on the development of a metallic core with a non-convex rotating unit geometry and a theoretical Poisson's ratio of -1. A Uniaxial Tensile Test was conducted to find the effective elastic properties of the Hybrid Material Structure. The results of this study showed that the Hybrid Laminate, a form of the Hybrid Structure, did not retain any auxetic characteristics found in its separate component, the Metal Core. This is contrary to the original theory used to develop these Hybrid Laminates, as the Hybrid Structure's Ultimate Poisson's Ratio increased rather than decreasing as expected. The results further demonstrate that the high in-plane stiffness of the Composite Face Sheets, when bonded together with other sheet layers in the Hybrid Structures, limits the rotational mechanism necessary for producing the auxetic effect. This finding concludes that for the hybrid Fiber Metal Laminates to achieve the auxetic characteristics inherent in their Metal Core components, the interface design must be such that enough freedom is allowed for geometric variations. The Guidelines established in this study are intended to assist in the development of next-generation Metamaterial Composite Fabrics with sufficient geometric freedom.

Keywords: fiber metal laminates (fml); auxetic materials; negative poisson's ratio; finite element analysis (fea); metamaterial composites; structural constraints.

1. Introduction

Due to combining the high strength-to-weight ratio offered by Fiber Reinforced Polymers (FRPs) with the tensile strength/durability and impact resistance of metals, Fiber Metal Laminates (FMLs) are gaining acceptance in sophisticated industries, including aerospace and automotive engineering. Manufacturers of FMLs have developed GLARE, which consists of glass laminated onto an aluminum alloy core with a two-part epoxy adhesive for structural support. Existing FML products typically use a solid sheet of metal to distribute loads, fill cracks, and extend the life expectancy of the composite under fatigue load conditions. As increasing numbers of engineers and designers attempt to build next-generation lightweight structures with superior energy absorption capabilities, an increasing number of engineering companies are investigating the use of Metamaterials to provide additional support and reinforcement to FML structures [1].

Negative Poisson's Ratio (NPR), also called auxetic materials, is one of the most interesting types of metamaterials. These types of metamaterials behave differently from traditional materials when they undergo tension. Instead of contracting laterally when being stretched, auxetic structures actually expand in the transverse direction. Because of this unique behavior, they have a greater shear modulus, a higher fracture toughness, and a different permeability than traditional materials [2]. Therefore, auxetic materials have been widely studied for use in impact-prone structures. However, research into the use of auxetic geometries in the metallic core of hybrid composite materials has not received as much attention as research into the use of auxetic foams and 3D lattice-like structures.[3]

Fiber Metal Laminates (FMLs) include E-glass/epoxy reinforced aluminum, which are common in Aerospace and Marine Engineering. Research has also shown that nearly two-thirds of all energy absorbed by an FML structure occurs through plastic deformation of the metal phase. Completion of these numbers has led many researchers who have performed numerical/existing work using FEA methods to concentrate on determining what the best stacking or lamination sequence is for improving the performance of an FML. Specifically, **C. M. Arndt** [4] found that the use of different combinations of fiber types (carbon vs glass) results in a significant difference in the collision integrity of an FML resulting from the same impact event, as determined by 3D FEA results.

Despite traditional marine and aerospace designs having limitations, the optimization of some of the cores' composite material combinations, **A. Caramatescu et al.,** [5] studied a hybrid 2's composite core - which reduced the overall displacements of core materials by close to 45%, but provided an 8.6% increase in weight) demonstrates a fundamental weight vs stiffness trade-off. In contrast, current cellular sandwich assemblies remain highly susceptible to impact damage, as the skins and cores have insufficient strength to prevent failure under these weight loads by **A. F. Johnson** [6]. Other studies that have investigated honeycomb core materials have strictly focused on how the physical characteristics of the core material affect the overall response of the sandwich assembly. (To determine the extent of the influence, researchers used statistical LogWorth analysis to identify materials sensitive to design changes, based solely on continuum beam theory). Thus, there is an urgent need to identify metamaterials suitable for sandwich construction.

The re-entrant honeycomb structure is currently the most researched auxetic structure and has demonstrated superior ballistic protection due to its ability to sustain extended inertia (NPR) during significant mechanical stress by **R. Mohamed et al.,** [7] . This structure provides the greatest ballistic protection against crushing forces supplied by a projectile because of the NPR effect. Other examples of auxetic structures exist and may exhibit similar mechanical characteristics, but through the exploitation of different configurations. For example, hexachiral Ti-6Al-4V lattices created using Selective Electron Beam Melting (SEBM) are chiral configurations by **N. Novak et al.** [8]. Additionally, double arrow-head geometries illustrate that the NPR effect induces material concentration at the tips of both arrows and leads to improved energy absorption characteristics studied by **Ganchao Chen et al.,** [9]. Three-dimensional re-entrant lattices have also been developed to provide through-the-thickness NPR as studied by **Rohit Raju Madke et al.**, [10] while elliptical hole arrays utilize instability mechanisms to achieve strain-dependent behavior studied by **K. Logakannan et al.,** [11]. Because there were many different configurations that can exhibit NPR behavior, mechanical responses can be tailored to meet specific applications that require energy absorption during an impact. **H. Al-Rifaie et al**. [12]developed an auxetic anti-ram bollard, capable of stopping an M1-class vehicle traveling at 64 km/h, which is at least double that of a standard hollow steel bollard, with an additional 52% increase in energy entered into the duty cycle. Additionally**, I. A. Shah et al.,** [13] research into auxetic sandwich armor also shows significant benefits; several studies have shown that structural integrity was maintained during impacts of velocities as high as 400 m/s.

The choice of face sheet material affects the performance of auxetic composite laminates. For example, steel face sheets have been used for applications that require blast resistance. The bonding method used with the steel face sheets has been the subject of several studies, such as, **Zicheng Yan et al.,** [14] with one study comparing 'adhesive vs integrated' bonding methods. Hybrid configurations that combine steel face sheets and CFRP face sheets have also demonstrated improved performance against ballistic impact (e.g., the ability of the auxetic core to increase the damage tolerance of an HSP by **Junbo Yan et al.,** [15] .

As such, advanced multifunctional face sheets that integrate magneto-electro-elastic properties can provide the ability to support coupled electromechanical functions, such as with smart structure applications. This allows for the "non-linear vibration analysis of laminated plates containing auxetic honeycomb core and magneto-electro-elastic face sheets", where it was assumed that the mechanical properties of the auxetic core, including the negative Poisson's ratio, are dependent upon the geometry of the unit cells and the elastic modulus of the original material by **Ngo Dinh Dat et al.,** [16].

Auxetic cores offer distinct benefits when isolated, although challenges remain about how to implement their integration into structural laminate systems. Testing of auxetic CFRP laminates found a 40% decrease in the amount of tensile damage sustained, but an overall lower level of energy loss than traditional CFRPs by **Y. Wang** [17] . The evidence suggests that Fibre-based auxetic properties alone do not provide sufficient energy absorption capabilities for applications with high impact loads. Several studies of lattice structures with hybrid/sandwich construction, such as **R. Wang et al.**, [18]indicate that integrating an auxetic frame with a ceramic filling significantly (up to 73%) reduces the amount of volume loss due to impacts. Although documentation exists identifying the unique characteristics of these impacts due to the lattice frames, there remains a gap in the knowledge of fully understanding the relationships between the auxetic lattice frames and the infill matrix.

Research using numerical simulations of composite annular plates has demonstrated that using auxetic faces increases the maximum critical buckling loads that can be subjected to these plates as by **D. Pawlus** [19]. However, these studies used only soft foam cores or theoretical Finite Difference models for their evaluations. Conversely, different methods using Shape Memory Alloys (SMA) employ complex pre-straining, phase changes, or some combination of pre-straining and phase changes, instead of making use purely of the geometric characteristics of Shape Memory Alloys, as a structuring approach [20]. Researchers predominantly utilize a Finite Element Analysis approach for numerical investigations of auxetic composite laminates through specialized software programs. The Finite Element Analysis approach that is most-used when researching dynamically loaded cases is LS-DYNA, with the load blast enhanced (Conwep method), Smooth Particle Hydrodynamics (SPH) method, and Multi-Material Arbitrary Lagrange-Eulerian (MMALE) method, utilized for the simulation of blast loading by **N. Novak et al.,** [21]. The explicit dynamic nature of LS-DYNA permits precise simulation of high-strain-rate events through application of the “Johnson-Cook model” to simulate rate-dependent behavior of materials.

Furthermore, integration of ANSYS/LS-DYNA has been used successfully in studies evaluating compression properties of auxetic composites using solid elements (ELFORM = 1) for auxetic components, and TSHELL elements of ELFORM = 5 were utilized for evaluating the compressive properties of conventional composite structures as studied by **K. Logakannan et al.,** [11]. In addition to the above software integration, various other software programs have been utilized to conduct specialized types of analytical methodologies. For example, Siemens NX 12.0 Nastran has been used to conduct buckling analyses using Tetra10 elements with a size of 0.2 mm as studied by **P. Sengsri et al.,** [22].

The physical restrictions set by laminate construction represent the greatest deficiency in existing literature. In other words, the auxetic effect depends on the ability of a unit cell to be able to rotate and deform with respect to its surrounding matrix. However, when this unit cell is

embedded inside of hybrid Fibre Metal Laminates (FML), these weaves are bonded to the metal core with solid resin, providing no relative motion between these outer skins of glass or carbon fibre and the resin matrix. To date, there are no published studies showing how current literature regarding the effects of rigid outer layers of resin on a continuous auxetic Steel sheet will affect the geometric freedom associated with the continuous behaviour of the auxetic. Therefore, it is currently uncertain whether the negative Poisson's ratio could remain intact or if it could be negated by being constrained by highly stiff skins.

This research explored a composite laminate consisting of a perforated metamaterial sheet of steel located between layers of glass fibre reinforced plastic (GFRP) and carbon fibre reinforced laminate (CFRP). By employing Finite Element Analysis (FEA) on Abaqus software, we have modelled the impact of nonconvex voided geometries upon the elastic modulus and Poisson's ratios of the completely bonded laminate. In contrast to previous investigations that concentrated on stand-alone sheets or flexible foamed materials, our study targets the constraint mechanism, thereby generating significant design limitations for hybrid metamaterial laminates.

2. Research Materials and Methods

2.1 Metamaterial Unit Cell Design

In the present investigation, the study's auxetic metamaterial sheet was developed using the original concept of a bean-shaped perforation, as proposed by Wang et al. [39], wherein a periodic structure is produced that has a very low Poisson's ratio under uniaxial compression. The objectives of the metamaterial core included maximizing the amount of porosity while preserving its auxetic behaviours, thus producing an overall decrease in the structural weight of the hybrid composite laminate containing it. The unit cell has a geometric configuration of an array of bean-shaped voids that are formed from the overlap of circular arcs that are arranged in a periodic pattern. The unit cell's primary geometric parameters are shown in Figure 1 below and Table 1 below; these parameters were selected using previously reported parametric studies by Wang et al., which focused on configurations that exhibit the highest values for negative effective Poisson's ratios. Analytical geometric relationships were used to create the geometry of the unit cell. A Pythagorean relationship was used to determine the center position of the large arc to provide tangential continuity between arcs, creating a smooth Shape and Cylindrical bean-shaped cavity.

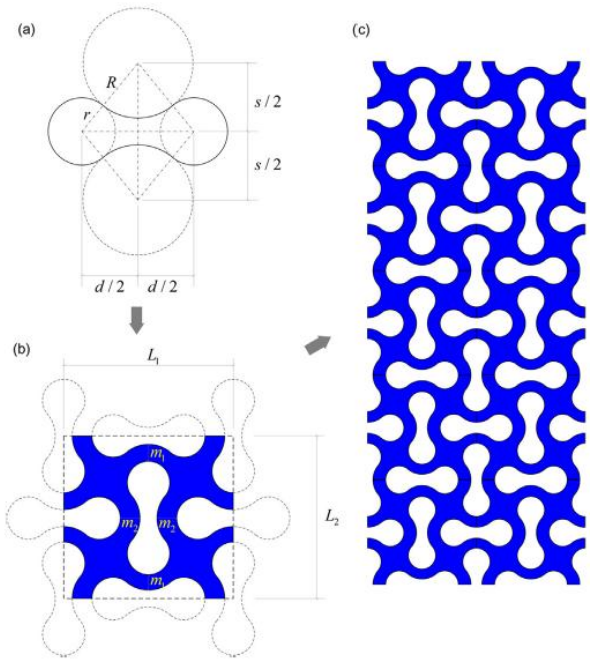

Fig.1: Proposed geometric structure of Wang et al. for a sheet with a negative Poisson's ratio a) bean holes b) core and c) a complete sheet [39]

Table 1: The geometric parameters of the metamaterial unit cell

Parameter	Description	Value (mm)
L_1, L_2	Unit cell dimensions	40
R	Radius of large arc	20
r	Radius of small arc	6
d	Center distance	10
t	Sheet thickness	0.5

2.2 Geometric Construction and Numerical Evaluation of the Metamaterial Unit Cell

Abaqus/CAE was utilized to produce the 3D solid model of the metamaterial unit cell through the development of a new deformable 3D component created as a representation of the metamaterial unit core cell. A rectangular domain of dimension (L×L=40×40mm). It was established to initiate the geometric model development. In addition, there were two circular arc profiles of radius (r=6mm), centered symmetrically within the square area and separated at (d=20mm), (i.e., center to center). The larger circular arc was added to create a narrowing effect of the characteristic bean-shaped cavity. To find the vertical separation of the circular arc, the Pythagorean theorem was used.

$$h = \sqrt{(r + \frac{d}{2})^2 - (\frac{d}{2})^2} \qquad (1)$$

$$h = \sqrt{(6 + 10)^2 - 10^2} = 12.49\ mm$$

Figure 2 (a) shows how the initial geometric design of the metamaterial unit cell is created using overlapping circular arcs. To create the next step, we need to eliminate all redundant portions of the large circle so only the curved back portion that creates the narrowing of the bean-shaped cavity is left. Once this is done, we then copy that portion of the design and flip it vertically with respect to the x-axis, and finally remove the interior regions of the small circles. The process results in a smooth symmetric shape that forms a complete continuous bean-shaped cavity as shown in Figure 2 (b).

Afterward, a single bean cavity duplication will yield two-dimensional metamaterials with a two-dimensional periodic unit cell that can be seen in Figure 2 (c) by both rotational replications, followed by translation to produce the periodic unit cell. The resultant two-dimensional geometric layout is extruded perpendicular to the two-dimensional plane so that it becomes a three-dimensional metamaterial unit cell having a uniform thickness of 0.5 millimeters (Figure 2 (d)).

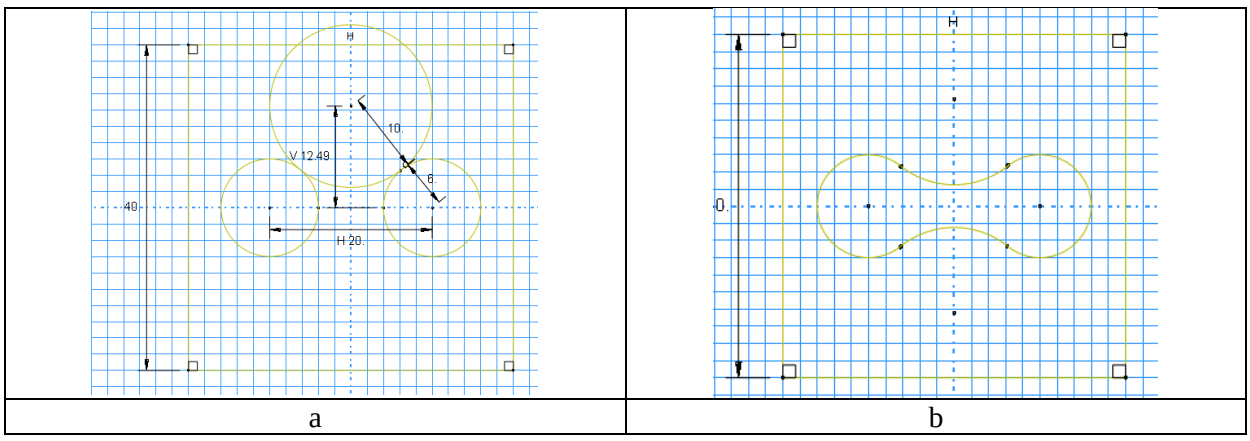

a b

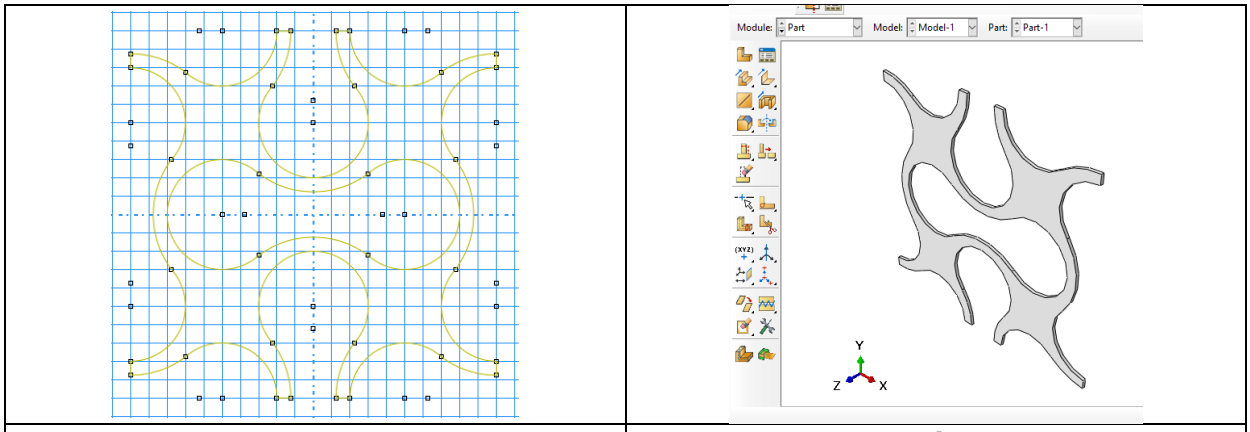

c d

Fig. 2. Geometric construction procedure of the metamaterial unit cell: (a) initial arrangement of circular arcs used to generate the base geometry; (b) trimming and reflection of overlapping regions to form the bean-shaped cavity; (c) periodic replication and rotation of the cavity to generate the two-dimensional base cell; (d) three-dimensional unit cell obtained by extrusion with a uniform thickness of 0.5 mm.

Before the entire metamaterial structure was constructed, the single unit cell from the metamaterial was tested under uniaxial tension to check for auxetic behaviour. The arrangement of the loading and boundary conditions for a single unit cell can be seen in Figure 3. The upper boundary, uy = 5mm, has a pre-defined movement. The lower boundary is constrained in the y-direction, but it is free to move along both the x and z axes. The left side of the boundary is attached in both the x and z directions only; it can slide up or down along the y-axis without restriction on either movement. The right side of the boundary can move freely. This configuration will allow for a lateral deformation of the unit cell, while still preventing any rigid-body movement. The base material for the unit cell was considered to be linear steel with a modulus of elasticity, E = 200 GPa, and a ratio of Poisson's, ν = 0.23. The deformation pattern from the uniaxial tensile testing in Figure 4 clearly illustrates axial stretch in the direction of load and transverse lateral expansion, which is an important defining characteristic of auxetic materials. The effective Poisson's ratio has been calculated, using the average strain components from the metamaterial unit cell as follows:

$$\nu = -\frac{\varepsilon_{xx}}{\varepsilon_{yy}} = -1 \qquad (2)$$

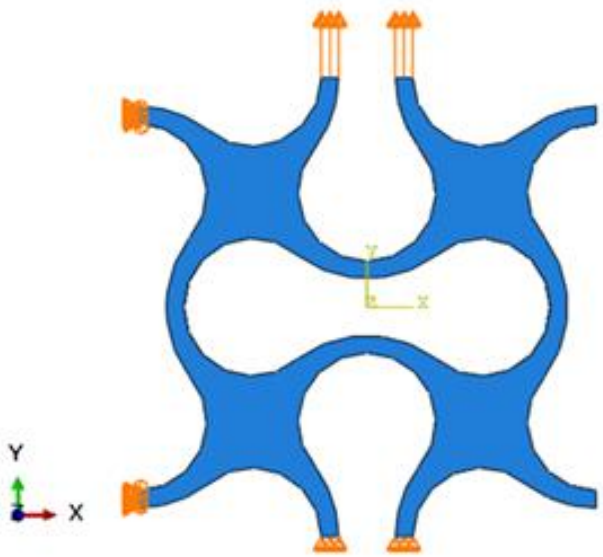

Fig.3: Boundary condition and uniaxial displacement loading on metamaterial unit cell.

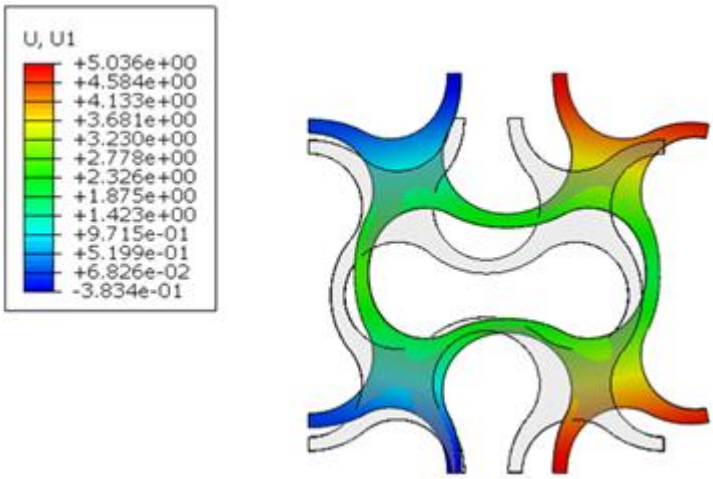

Fig.4: Unit cell deformation under uniaxial tension for auxetic behavior.

2.2.1 Evaluation of Porosity and Effective Density

The porosity of the metaloid cellular unit was determined using a ratio of total void area compared to the cellular unit's area. By definition, this porosity can be defined by the relationship: And the following relationship:

$$\phi = \frac{4A}{L^2} \qquad (3)$$

Where A is equal to the area of the individual cellular bead (bean shaped cavity) as follows:

$$A = 2\pi r^2 + \frac{ds}{2} - 2R^2 \arcsin\left(\frac{d}{2(R+r)}\right) - 2r^2 \arccos\left(\frac{d}{2(R+r)}\right) \quad (4)$$

Where d = a single cavity; D = diameter of the outermost cavity in the half section of the bead. The effective density of the metaloid sheet was calculated using:

$$\phi = \frac{4\times 276.47}{40^2} = 0.69 \qquad (5)$$

And the density of the metamaterial sheet will be equal to:

$$\rho^* = (1-\phi)\rho = 0.31\rho \quad (6)$$

Assuming a steel density of ρ=7800kg/m3, the resulting bottleneck is equal to ρ*= 2403kg/m3 (substantial reduction in density and very high negative value of Poisson's Ratio for Metaloid Sheet). These findings indicate that the geometry of the metaloid sheet allows for significant weight savings and still possesses a negative Poisson's Ratio that is advantageous for future use as hybrids, thus making it highly applicable for use as an alternate lightweight composite material in manufacturing.

2.2.2 Decreasing the Density of Metamaterial Sheets

Composite and metamaterial-based designs are often employed with the aim of minimizing the weight of a structure, yet maximizing its mechanical performance. For instance, if a metamaterial sheet were created using steel as the base material, the goal of reducing the density would be an important aspect of this design. To achieve this design goal, specific areas of each unit cell (that support lower stress levels) would be targeted for material removal. This is accomplished by creating circular holes at predetermined locations within each metamaterial cell (as shown in the modified unit-cell geometry in Figure 5). With this design approach, the overall mass of the structure is decreased while still retaining an auxetic behaviour. The introduction of four holes within each unit cell yields a density reduction of approximately 16% with minimal reduction in the negative Poisson's ratio. In this example, the effective Poisson's ratio for the optimized cell was determined as follows:

$$\nu^* = -0.98$$

To calculate the density, the parameter A is modified as follows:

$$A = 2\pi r^2 + \frac{ds}{2} - 2R^2 \arcsin\left(\frac{d}{2(R+r)}\right) - 2r^2 \arccos\left(\frac{d}{2(R+r)}\right) + \pi r_{hole}^2 \qquad (7)$$

In this case, the density will be equal to:

$$\rho^* = 2020 \frac{kg}{m^3}$$

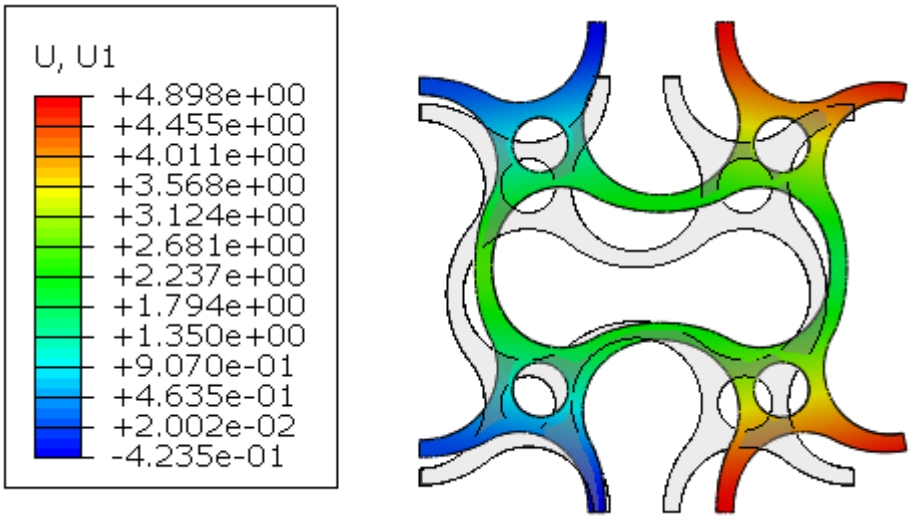

Fig.5: Metamaterial unit cell modified for weight reduction.

2.3 Modeling of the Complete Metamaterial Sheet

To be able to produce the entire metamaterial sheet during the sketching process, an array of 4 x 4 units was created by copying and connecting together all of the basic unit cells. Geometric tolerances can result in mismatches and very small distance gaps at the intersections between the adjacent cells. These differences may create a Geometric error message from the software. The left-side toolbar has Tools that repair the geometric error and create constraints to produce proper alignment and continuity.

The complete metamaterial sheet that was produced is shown in Figure 6 at an overall size of 160 by 160 mm; and the deformation of the metamaterial sheet when exposed to unidirectional tensile loads is illustrated in Figure 7.

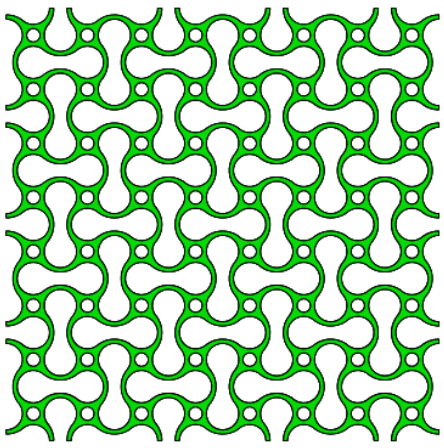

Fig.6: Full metamaterial sheet (160 × 160 mm) created by a 4 × 4 unit-cell lattice.

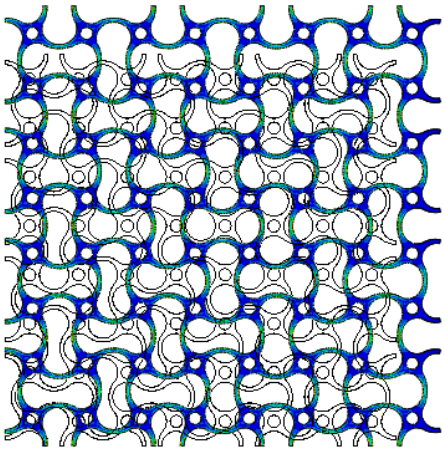

Fig.7: Unidirectional traction loading and deformation of the metamaterial sheet.

3. Composite Sheet Modeling

A shell formulation was used to create a Composite Sheet. The Shell is a flat component with the same dimensions as the Composite (metamaterial). This happens to the surface, too.

3.1 Properties of Composite Material

Homogeneous Orthotropic Elastic is used to define composites. An orthotropic composite contains three orthogonally positioned symmetries to the material and is suitable for use in unidirectional fibre reinforcement. The orthotropy of ABAQUS will be defined in this model by a stiffness matrix with its matrix components as follows:

Create Material → Mechanical → Elasticity → Elastic → Type: Orthotropic

[D1111= ;D1122= ; D2222= ; D1133= ; D2233= ; D3333= ; D1212= ; D1313= ; D2323=]

According to the instructions of the Abacus software, the coefficients of the hardness matrix are related to the required data of the Abacus as:

$$\begin{gathered} D_{1111} = C_{11}, D_{1122} = C_{12}, D_{1133} = C_{13}, \\ D_{2222} = C_{22}, D_{2233} = C_{23}, D_{3333} = C_{33}, \\ D_{1212} = C_{44}, D_{1313} = C_{55}, D_{2323} = C_{66} \end{gathered} \tag{8}$$

C-ij. Matrix coefficients are hardness and indicate the stress-strain relationship:

$$\begin{Bmatrix} \sigma_L \\ \sigma_T \\ \sigma_N \\ \tau_{LT} \\ \tau_{LN} \\ \tau_{TN} \end{Bmatrix} = \begin{bmatrix} C_{11} & C_{12} & C_{13} & 0 & 0 & 0 \\ C_{12} & C_{22} & C_{23} & 0 & 0 & 0 \\ C_{13} & C_{23} & C_{33} & 0 & 0 & 0 \\ 0 & 0 & 0 & C_{44} & 0 & 0 \\ 0 & 0 & 0 & 0 & C_{55} & 0 \\ 0 & 0 & 0 & 0 & 0 & C_{66} \end{bmatrix} \begin{Bmatrix} \varepsilon_L \\ \varepsilon_T \\ \varepsilon_N \\ \gamma_{LT} \\ \gamma_{LN} \\ \gamma_{TN} \end{Bmatrix} \tag{9}$$

The subscript L shows the fiber direction, T and N directions perpendicular to the fibers. Therefore, it can be concluded that for a single-layer composite, the characteristics of the composite plate are the same in N and T directions, and this is a transversely isotropic material.

$$C_{22} = C_{33}, C_{12} = C_{13}, C_{44} = C_{55}, C_{66} = (C_{22} - C_{23})/2 \tag{10}$$

According to these relations, the number of independent constants in this stress-strain relationship decreased to 5.

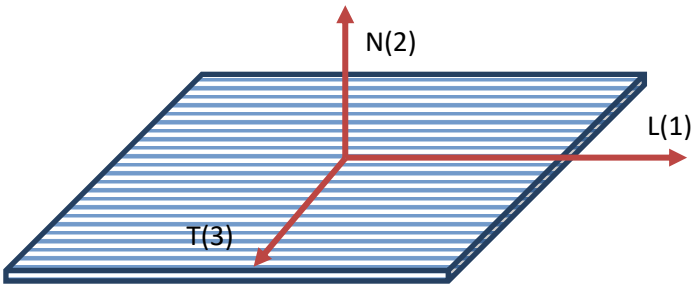

Fig.8: The ABAQUS software analyzes the directional properties (MODULI).

These constants and engineering functions for one orthotropic material are related to each other.

$$C_{11} = \frac{1-\nu_{23}\nu_{32}}{E_2E_3\Delta}, C_{22} = \frac{1-\nu_{13}\nu_{31}}{E_1E_3\Delta}, C_{33} = \frac{1-\nu_{12}\nu_{21}}{E_1E_2\Delta}, \quad (11)$$

$$C_{12} = \frac{\nu_{21}+\nu_{31}\nu_{23}}{E_2E_3\Delta} = \frac{\nu_{12}+\nu_{13}\nu_{32}}{E_1E_3\Delta}$$

$$C_{13} = \frac{\nu_{31}+\nu_{21}\nu_{32}}{E_2E_3\Delta} = \frac{\nu_{13}+\nu_{12}\nu_{23}}{E_1E_2\Delta}$$

$$C_{23} = \frac{\nu_{32}+\nu_{12}\nu_{31}}{E_1E_3\Delta} = \frac{\nu_{23}+\nu_{21}\nu_{13}}{E_1E_2\Delta}$$

$$C_{44} = G_{23}, C_{55} = G_{31}, C_{66} = G_{12}$$

$$\Delta = \frac{1-\nu_{12}\nu_{21}-\nu_{23}\nu_{32}-\nu_{31}\nu_{13}-2\nu_{21}\nu_{32}\nu_{13}}{E_1E_2E_3}$$

In addition, the symmetry in the behavior of an orthotropic material is the following:

$$\frac{\nu_{ij}}{\nu_{ji}} = \frac{E_i}{E_j} \quad (12)$$

For example: $\nu_{21} = \nu_{12}\frac{E_2}{E_1}$.

And for a perpendicular-isotropic material, the engineering constants are:

$$E_2 = E_3, \nu_{12} = \nu_{13}, G_{12} = G_{31} \quad (13)$$

Also, since this material is isotropic, the relationship between Young's modulus, Poisson's ratio, and the shear modulus of isotropic materials is also maintained:

$$G_{23} = \frac{E_2}{2(1+\nu_{23})} \qquad (14)$$

In this study, the following engineering material constants are considered for carbon fibers.

Table 2: The engineering constants of the carbon fiber composite

E_1 MPa	$E_2 = E_3$ MPa	$G_{12} = G_{13}$ MPa	$\nu_{12} = \nu_{13}$	$\nu_{23} = \nu_{32}$
145880	13312	4386	0.263	0.470

To calculate values D_{ijkl} if needed, we first calculate other values ν_{ij} of engineering constants with the help of relations (12) to (14). Therefore, we will have:

$$\nu_{31} = \nu_{21} = \nu_{12}\frac{E_2}{E_1} = 0.263 \times \frac{13312}{145880} = 0.024$$

$$G_{23} = \frac{E_2}{2(1+\nu_{23})} = \frac{13312\ MPa}{2(1+0.470)} = 4528\ MPa$$

And therefore, the constant values to be included in the software will be as follows:

Table 3: Constant values of properties of unidirectional orthotropic carbon fiber composites (MPa)

D1111	D1122	D2222	D1133	D2233	D3333	D1212	D1313	D2323
148209	6711	17249	6711	8268	17249	4386	4386	4528

The above method is used to calculate the constant coefficients of glass fiber composites, the results of which are shown in the tables below.

Table 4: Values of mechanical properties for unidirectional glass fibers

E_1 MPa	$E_2 = E_3$ MPa	$G_{12} = G_{13}$ MPa	$\nu_{12} = \nu_{13}$	$\nu_{23} = \nu_{32}$
37880	9407	3405	0.299	0.422

Table 5: Property constants of unidirectional orthotropic glass fiber composites (MPa)

D1111	D1122	D2222	D1133	D2233	D3333	D1212	D1313	D2323
39859	5120	11777	5120	5349	11777	3405	3405	3307

By defining the properties of the composite, we attribute these properties to the composite. Since a composite is not an isotropic material, it is necessary to determine the main directions of the material. For this purpose, the assign material orientation command is selected.

Composite layers are defined with the following command:

Properties>Create section> shell>composite

A window will open as shown below. Individual layers are defined in this window. In this page, the material, the angle of the fibers, the thickness of the layers, and the number of integration points are specified. Selecting the symmetric layers option, the composite layers are modeled symmetrically. The lowest layer of the composite is placed in the first row. In the figure below,

each sheet has 2 layers, each layer is defined as 0.5 mm thick. In the following, the method of modeling a metamaterial sheet and also how to combine it with a composite sheet will be examined.

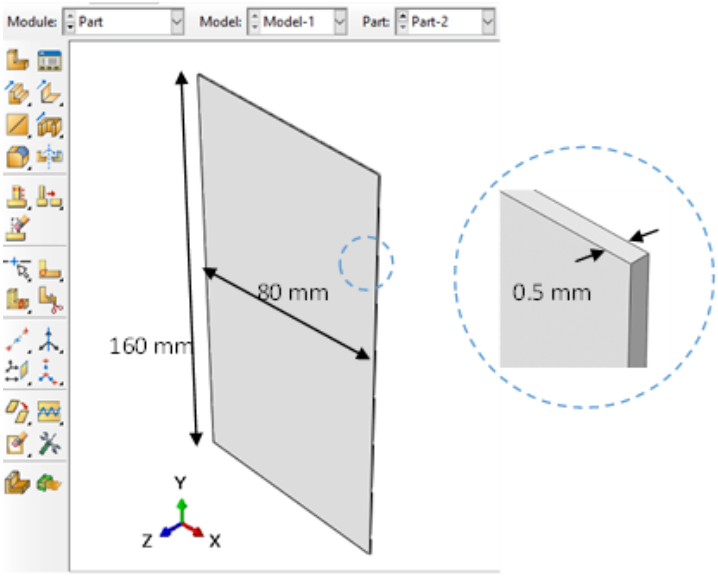

Fig.9: Composite sheet dimensions

3.2 Hybrid Composite Sheet

In order to fabricate the hybrid composite sheet, we use the "Tie" constraint to bond the two composite shell layers of the hybrid composite sheet to the metamaterial core. We define the Tie constraint via the following path in ABAQUS:

Create Interaction, Create Constraint, Tie.

Because the metamaterial sheet has a mesh size that is smaller than that of the composite flat sheets, we select the surface of the composite sheet as the Master Surface, and we define the surface of the metamaterial sheet as the Slave Surface. This decision provides stability and accurately provides displacements between the two components numerically. Because two composite layers are attached symmetrically to both sides of the metamaterial sheet to maintain symmetrically the structure, we apply the Tie constraint to both sides of the metamaterial sheet as well, so the total thickness of the hybrid composite sheet becomes 1.5 mm.

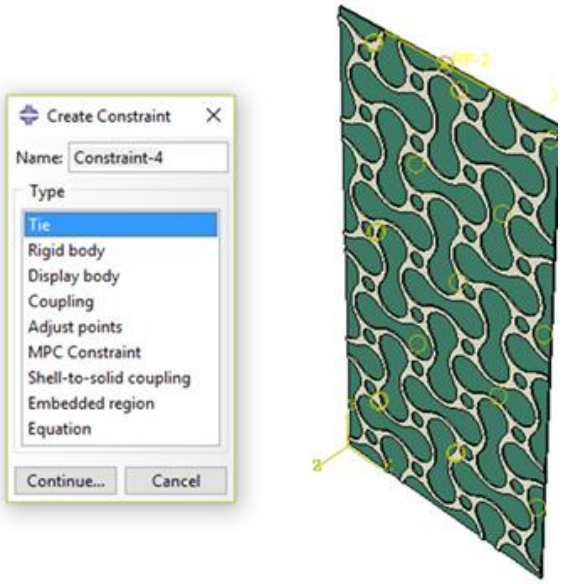

Fig.10: Definition of the Hybrid Composite State (Elastic Slab + Metamaterials) as a Function of Relative Orientation of the Two Layers.

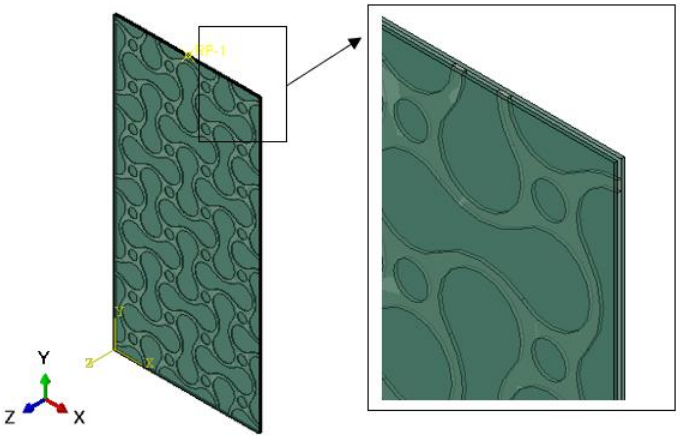

Fig.11: A hybrid composite configuration made of two composite layers, with each bonded symmetrically on either side of the metamaterial sheet.

3.3 Boundary conditions of the hybrid composite sample

The mechanical response of hybrid laminated composites occurs because they are composed of hybrid materials such as carbon and glass reinforcement, as well as various resins. The stiffness of these hybrid laminated composites is determined by their composite layer thickness and the volume fraction of each material. As previously mentioned, it is possible to determine the rigidity of hybrid laminated composites using a coupled loading technique. In this technique, the point at which the load is applied is referred to as the anchor point, which is placed at the centroid (i.e., halfway) of the cross-section of the hybrid plate cross-section. The anchor point is connected to all nodes in the hybrid plate and, as such, the load is applied to the anchor point, which transmits the load to all the nodes. Because the load will not be uniformly distributed across the surface of the hybrid plate, it is important that the anchor point is located correctly. Therefore, by maintaining the positioning of the anchor point at the centre of the cross-section of the hybrid plate, all nodes are constrained to follow the displacement of the anchor point. Hence, even when the displacement at the anchor point is prescribed in one direction, all nodes on the hybrid plate cross-section will still move in the same direction (i.e., as the anchor point is displaced).

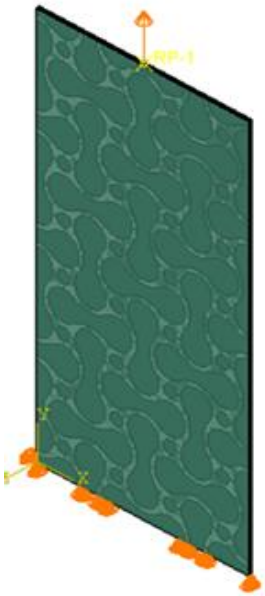

Fig.12: Boundary conditions of hybrid composite sheet.

3.4 Meshing

The metamaterial's mesh consisted of eight-node linear brick elements with reduced integration (C3D8R), and the average mesh size was 0.6 mm, which was used for the dimensions of the metamaterial unit cell. As shown in the following figure, this is the meshed metamaterial sheet.

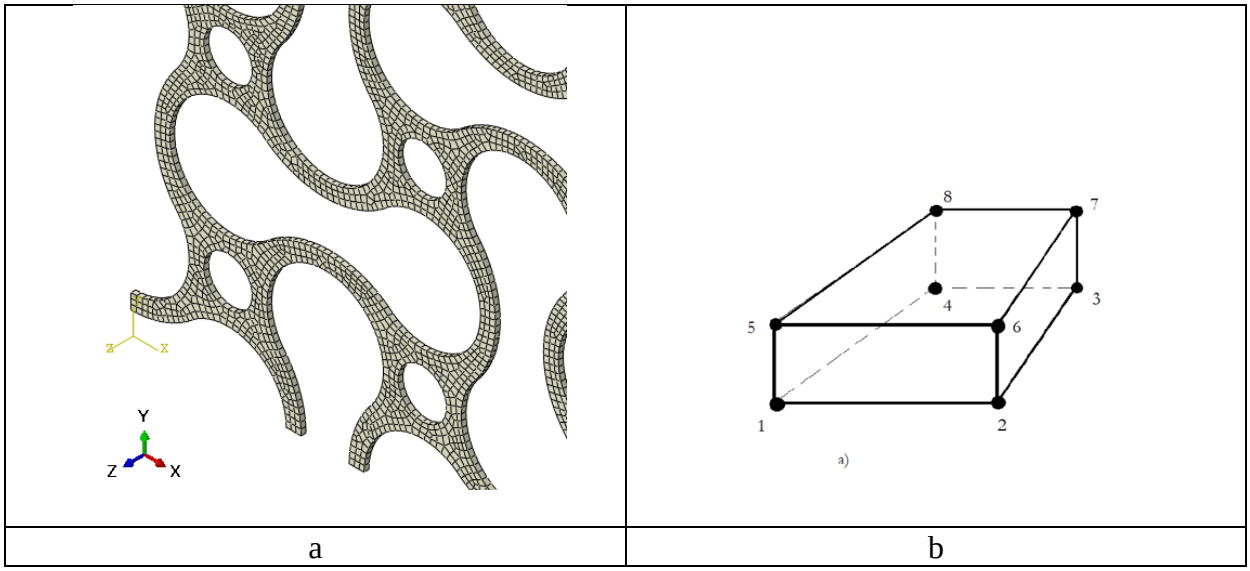

a b

Fig.13: (a) Meshing of a metamaterial sheet (b) C3D8R Eight-node Brick Element

The composite sheets were similarly meshed using the same element type (C3D8R), ensuring compatibility at the co-meshed Tie interface. Coarser meshes were used for the composite sheet layers, with an average mesh size of 1 mm.

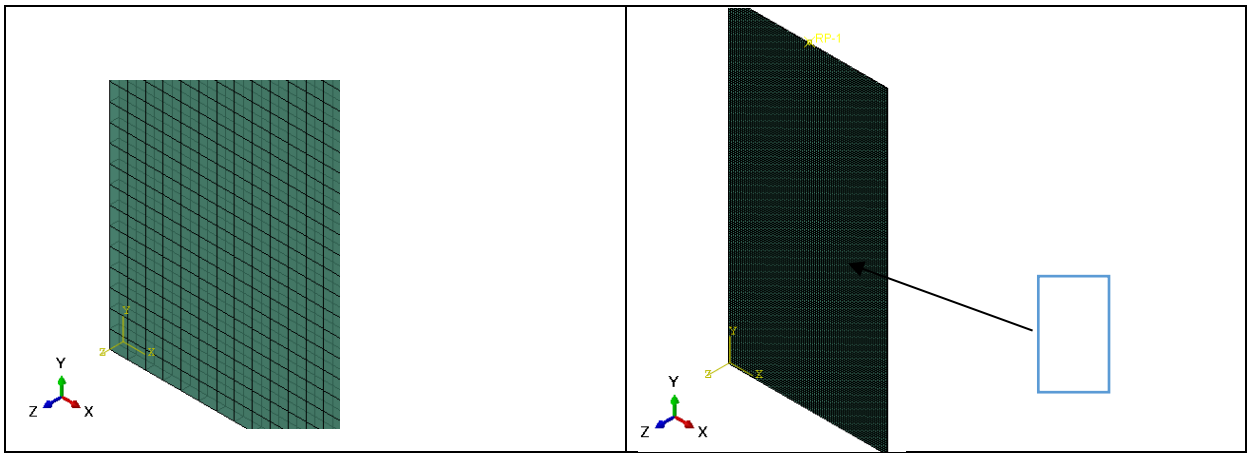

Fig.14: Composite sheet mesh average size 1 mm

4. Results and discussions

The inverse Poisson's ratio of auxiliary metamaterials causes lateral deformation to occur in the opposite direction to what is typically seen with composite materials, which have a positive Poisson's ratio. When combined with conventional composite layers, it is expected that the opposing axial deformation modes of the two types of materials would provide an increase in the overall stiffness and modify the hybrid structural response. This section first describes the numerical results for hybrid composite systems. The mechanical response of each of the steel metamaterial sheets, glass fiber composite sheets, and carbon fiber composite sheets is analyzed under uniaxial load separately. Then the impact of the metamaterial core on the mechanical properties of composite laminates is discussed by focusing on the development of stiffness characteristics and the behaviour of Poisson's ratio.

4.1 Simulation of the Metamaterials Sheet System

The metamaterials sheet has dimensions of 160 mm x 80 mm (2 x 4 directory), which has the same dimensions as the base's two unit cells for the design of the new system was the same method used above, as showed in the last chapter. The metamaterials will be load tested using unidirectional displacement loading and will be subjected to various boundary requirements.

Table 6: Loading results of a metamaterial sheet

reaction force Rf (N)	The maximum von Mises stressvon Mises (MPa)	Maximum vertical stress (MPa)	Maximum shear stress max (MPa)	The maximum displacement in the perpendicular direction (mm)
31.58	173.2	174.4	47.6	0.20

Due to displacement loading in$u_y = 0.4\ mm$ and also the above results, the average longitudinal strainε_{yy} and transverse strain $\varepsilon_{xx}$of this sheet is equal to:

$$\varepsilon_{yy} = \frac{u_y}{L_y} = \frac{0.4}{160} = 0.0025$$

$$\varepsilon_{xx} = \frac{u_x}{L_x} = \frac{0.20}{80} = 0.0025$$

And therefore, the Poisson's ratio is:

$$\nu = -\frac{\varepsilon_{xx}}{\varepsilon_{yy}} = -\frac{0.0025}{0.0025} = -1.0$$

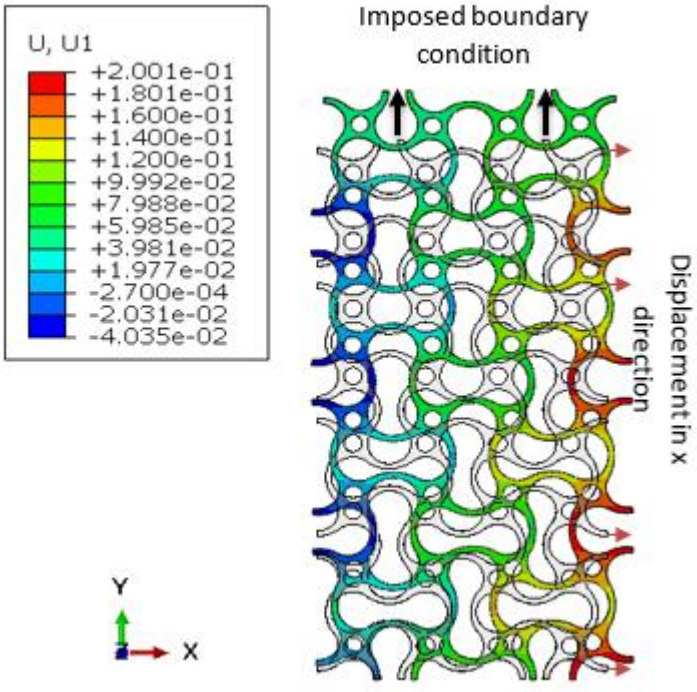

Fig.15: Moving the metamaterial sheet in the direction perpendicular to the loading (magnification of the image = 40)

Using the reaction force obtained $R_f = 31.58N$ from the simulation, the average elastic modulus of the object can be obtained:

$$\sigma = \frac{R_f}{A} = \frac{31.58N}{0.5 \times 80\ mm^2} = 790\ kPa$$ Average stress

$$E = \frac{\sigma}{\varepsilon_{yy}} = \frac{790kPa}{0.0025} = 316\ MPa$$ Young's modulus

As the calculations above show, the elastic modulus of steel is reduced from 200GPa to 316 MPa by creating non-convex cuts and creating a metamaterial.

4.2 The Glass Fiber Composite Sheet Simulation

The Glass Fiber Composite Sheet Simulation is a finite element analysis of a unidirectional glass fiber composite sheet (orthotropic material) with a thickness of 0.5 mm and dimensions of 160 x 80 mm² subjected to the same load.

Table 7: Loading results of a unidirectional glass fiber composite sheet

reaction force Rf (N)	The maximum von Mises stress on Mises (MPa)	Maximum vertical stress (MPa)	Maximum shear stress max (MPa)	The maximum displacement in the perpendicular direction (mm)
3788	92.05	92	0	-0.06

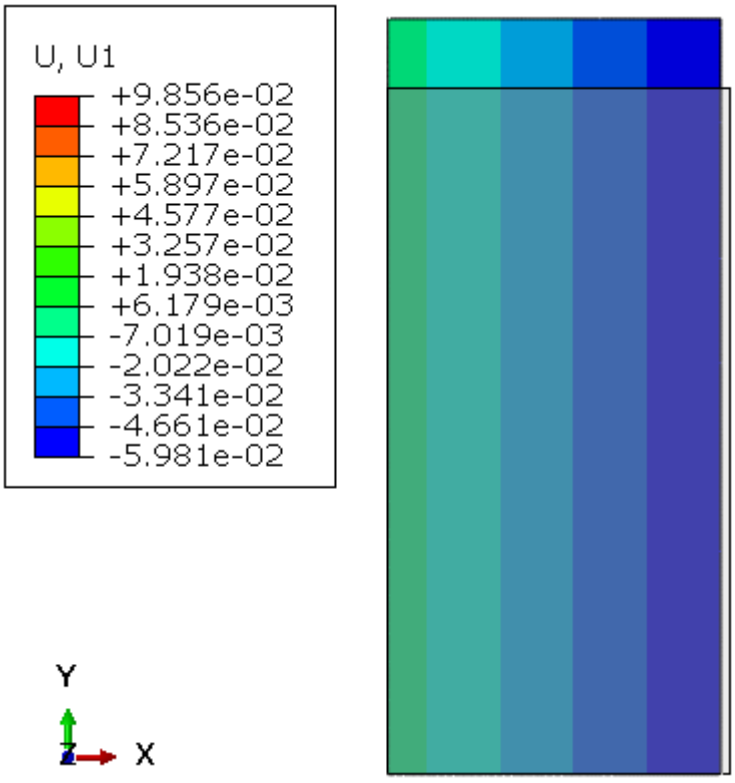

Fig.16: Moving the glass fiber composite sheet in the direction perpendicular to the load (magnification of the image = 40)

Given that the strain in the y direction is equal to$\varepsilon_{yy} = 0.0025$ and the strain in the x direction is equal to $\varepsilon_{xx} = -0.00075$ is, therefore, the value of Poisson's ratio in the composite sheet along 1-2 will be equal to:

$$\nu_{12} = -\frac{0.00075}{0.0025} = -0.3$$

which is equal to the value obtained in the third chapter.

The elastic modulus of glass fiber composite sheet is also obtained from the following relationship:

$$E = \frac{R_f}{\varepsilon_{yy} A} = \frac{3788}{0.0025 \times 40\ mm^2} = 37.88\ GPa$$

where A is the cross-sectional area of the composite. The obtained value is consistent with the value mentioned in section 3.

4.3 Simulation of carbon fiber composite sheet behavior

To study the behavior of the carbon fiber sheet, we do the same simulation done in the previous section for the glass fiber sheet. Here, also a sheet with a thickness of 0.5 mm and dimensions 160×80 mm^2 is considered and subjected to unidirectional displacement in the y direction and equal to u_y=0.4 mm, we put. The following table shows the results of this simulation.

Table 8: Loading results of a carbon fiber composite sheet

reaction force Rf (N)	The maximum von Mises stressvon Mises (MPa)	Maximum vertical stress (MPa)	Maximum shear stress max (MPa)	The maximum displacement in the perpendicular direction (mm)
14470	361.8	361.7	0	-0.0526

According to the obtained results, the elastic modulus of the carbon sheet in the loading direction is equal to:

$$E = \frac{R_f}{\varepsilon_{yy} A} = \frac{14470}{0.0025 \times 40\ mm^2} = 144.70\ GPa$$

Poisson's ratio of the carbon sheet in the direction perpendicular to the loading direction will be as follows:

$$\nu_{yx} = -\frac{\varepsilon_{xx}}{\varepsilon_{yy}} = \frac{6.575}{25} = 0.263$$

4.4 Simulation of a glass fiber composite sheet

According to the method mentioned in the third chapter, the modeling of the combined composite sheet with the metamaterial sheet is investigated. In this simulation, different combinations of composite sheets and metamaterial sheets are used. The purpose of this modeling is to investigate the effect of combining a metamaterial with composites. In the first modeling, two composite sheets and one metamaterial sheet are used. The following table shows the result of hybrid composite loading.

Table 9: Loading results of a combined composite sheet, including two glass fiber composite sheets and a metamaterial

Reaction force Rf (N)	The maximum von Mises stress on Mises (MPa)	Maximum vertical stress (MPa)	Maximum shear stress max (MPa)	The maximum displacement in the perpendicular direction (mm)
9310	488	487	159	-0.071

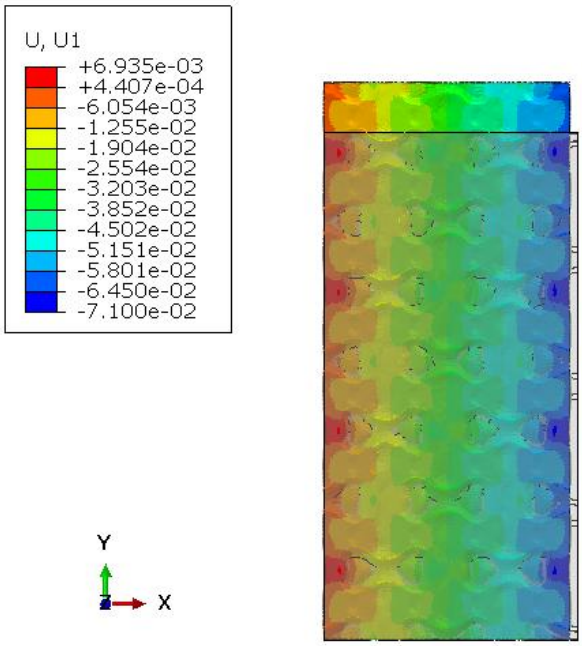

Fig.17: Displacement in the direction perpendicular to the loading direction in the combined composite sheet (two glass fiber sheets and one metamaterial sheet)

The result of this simulation shows that the strain in the direction perpendicular to the loading is not only not reduced but also increased with the presence of the metamaterial sheet.

$$\varepsilon_{xx} = -\frac{0.071}{80} = -8.875 \times 10^{-4}$$

As a result, contrary to expectation, Poisson's ratio will be positive and equal to:

$$\nu = -\frac{\varepsilon_{xx}}{\varepsilon_{yy}} = -\frac{-8.875}{25} = 0.355$$

In the figure below, the stress distribution along the y direction σ_{yy} it has been shown.

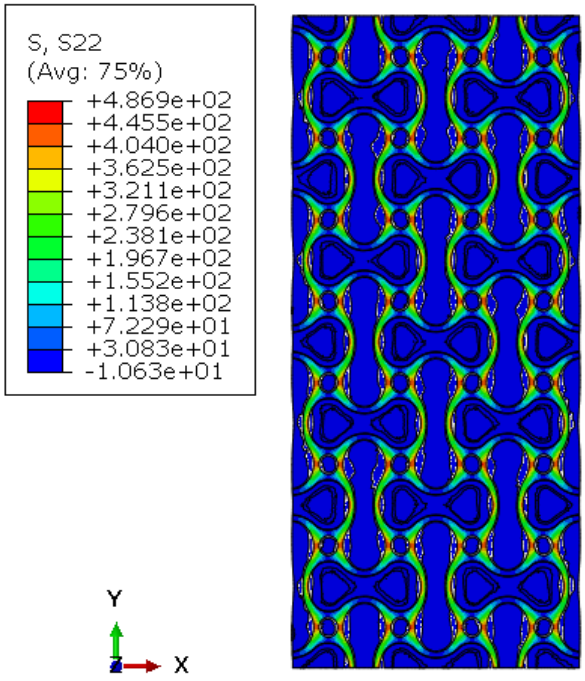

Fig.18: Tension σ_{yy} in hybrid composite sheet (two glass fiber sheets and one metamaterial sheet). To see the stress distribution, one of the composite plates has been removed from the display.

4.5 Simulation of a combined carbon fiber composite sheet

In this section, we will deal with the simulation of a hybrid composite made of two sheets of carbon fibers and one sheet of metamaterial. Similar to the previous example, a metamaterial sheet is placed between two composite sheets (here, carbon fibers). Then moving $u_y = 0.4\,mm$ it is applied to the upper surface of the sheets. The result of moving the points is shown in the figure below.

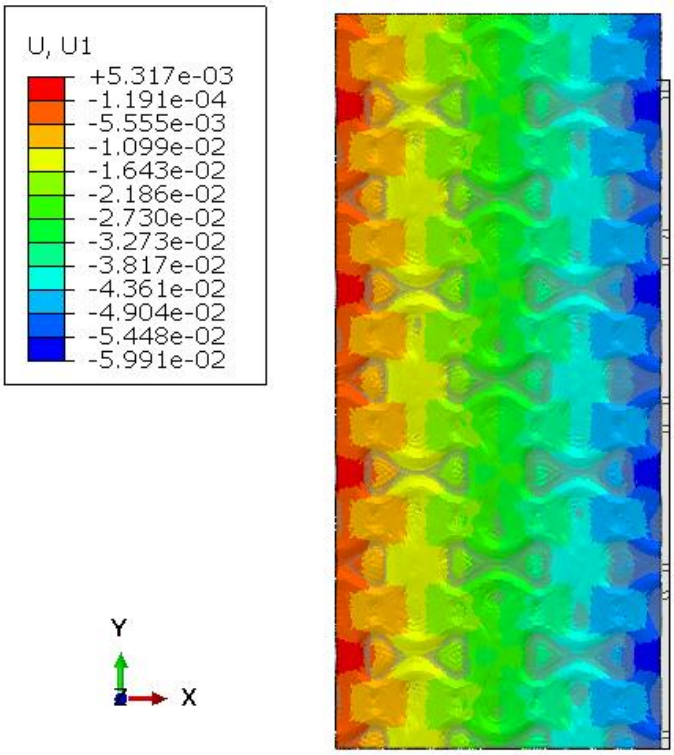

Fig.19: Displacement in the x direction related to a hybrid composite with two carbon sheets and one metamaterial sheet.

Table 10: Loading results of a hybrid composite sheet made of two carbon fiber composite sheets and a metamaterial

reaction force Rf (N)	The maximum von Mises stress on Mises (MPa)	Maximum vertical stress (MPa)	Maximum shear stress max (MPa)	The maximum displacement in the perpendicular direction (mm)
31400	575	575	160	-0.06

According to these results, the presence of the metamaterial sheet had no effect on the Poisson's ratio of the composite, and the displacement of the plates in the direction perpendicular to the loading is almost equal to the displacement of the carbon fiber sheets, $u_x = -0.06\,mm$.

The Poisson's ratio of the composite sheet in the direction perpendicular to the loading direction will be as follows:

$$\nu_{yx} = -\frac{\varepsilon_{xx}}{\varepsilon_{yy}} = \frac{6.575}{25} = 0.3$$

The combination of metamaterial sheet with carbon fiber composites not only could not cause the Poisson's ratio of the composite sheet to become negative or decrease, but also increased it.

5. Conclusion

In this article, we present our findings from a study that looked into the mechanical performance of hybrid composite laminate systems with an auxetic core made from engineered metal, called a Metamaterial. The core design consists of a series of bean-shaped holes placed in a non-convex shape; this allowed us to significantly reduce the density of the core by 16% while still maintaining a very negative Poisson's ratio, which of approximately -1. However, this design change also led to a substantial decrease in the steel's effective modulus of elasticity, reducing it to ~316 MPa. Hybrid composites were created using layers of metal and two layers of fiber-reinforced composites (either glass fiber or carbon fiber). When analyzing the hybrid composites subjected to a unidirectional loading, we found that, surprisingly, the auxetic behaviour of the metamaterial core was not apparent at the warp-level of the composite laminate. For the glass composite hybrid, the effective Poisson's ratio increased from 0.30 to 0.355 when compared with an identical glass composite laminate without an auxetic core. For the carbon- composite hybrid, the effective Poisson's ratio remained very close to that of the carbon fibre composite laminate without an auxetic core with only a slight increase in the value.

The auxetic behavior of the metamaterial has been inhibited by its stiffened outer skins made of composite; the overall global deformative response is primarily determined by the composite layers. It is important for hybrid auxetic-composite combinations to have a compatible level of stiffness if one wishes to take advantage of the auxetics in a structural application. Therefore, different combinations of materials or thickness ratios would need to be contemplated.

References

1. J. Bieniaś, “FIBRE METAL LAMINATES-SOME ASPECTS OF MANUFACTURING PROCESS, STRUCTURE AND SELECTED PROPERTIES,” 2011.
2. B. TEPEHAN and İ. Y. SÜLÜ, “Mechanical Analysis of a Layered Hybrid Composite Plate Created for Helmet Structures,” *Bayburt Üniversitesi Fen Bilimleri Dergisi*, vol. 5, no. 1, pp. 69–80, Jun. 2022, doi: 10.55117/bufbd.1084327.
3. A. Alderson and K. L. Alderson, “Auxetic materials,” *Proceedings of the Institution of Mechanical Engineers, Part G: Journal of Aerospace Engineering*, vol. 221, no. 4, pp. 565–575, 2007, doi: 10.1243/09544100JAERO185.
4. C. M. Arndt, B. Heng, R. Butler, and S. C. Termaath, “Nondeterministic Parameter Space Characterization of the Damage Tolerance of a Composite/Metal Structure,” no. 4, pp. 485–514, Oct. 2022, doi: 10.48550/arXiv.2210.14054.
5. A. Caramatescu, I. Mocanu, and A. Modiga, “A New Concept of Composite Material for High Speed Boats,” *Materiale Plastice (Mater. Plast.)*, vol. 56, no. 1, pp. 11–17, 2019, doi: 10.37358/MP.19.1.5114.
6. A. F. Johnson, “Novel Hybrid Structural Core Sandwich Materials for Aircraft Applications,” pp. 9–11, Sep. 2008, doi: elib.dlr.de/56748/1/E-J_Symp_Porto_Johnson.
7. R. H. Mohamed, S. M. Lawaty, and A. M. A. El-Butch, “BALLISTIC IMPACT RESPONSE OF AN ALUMINUM SANDWICH PANEL WITH AUXETIC HONEYCOMB CORE STRUCTURE,” 2016. [Online]. Available: https://api.semanticscholar.org/CorpusID:199178305
8. N. Novak, L. Starevi, M. Vesenjak, and Z. Ren, “Blast and ballistic loading study of auxetic composite sandwich panels with LS-DYNA,” 2019. [Online]. Available: https://api.semanticscholar.org/CorpusID:201697226
9. G. Chen, Y. Cheng, P. Zhang, J. Liu, C. Chen, and S. Cai, “Design and modelling of auxetic double arrowhead honeycomb core sandwich panels for performance improvement under air blast loading,” *Journal of Sandwich Structures and Materials*, vol. 23, pp. 3574–3605, 2020, [Online]. Available: https://api.semanticscholar.org/CorpusID:225705300

10. R. R. Madke and R. Chowdhury, “Anti-impact behavior of auxetic sandwich structure with braided face sheets and 3D re-entrant cores,” *Composite Structures*, vol. 236, p. 111838, 2020, [Online]. Available: https://api.semanticscholar.org/CorpusID:214155443
11. K. P. Logakannan, J. Rengaswamy, S. Kumar, V. Ramachandran, and D. Ruan, “Mechanical response of a novel hybrid tube composed of an auxetic outer layer,” *Thin-Walled Structures*, vol. 171, Feb. 2022, doi: 10.1016/j.tws.2021.108649.
12. H. Al-Rifaie and A. Hassan, “Improving the Impact Resistance of Anti-Ram Bollards Using Auxetic and Honeycomb Cellular Cores,” *Applied Sciences (Switzerland)*, vol. 14, no. 19, Oct. 2024, doi: 10.3390/app14198898.
13. I. A. Shah *et al.*, “Finite Element Analysis of the Ballistic Impact on Auxetic Sandwich Composite Human Body Armor,” *Materials*, vol. 15, no. 6, Mar. 2022, doi: 10.3390/ma15062064.
14. Z. Yan, Y. Liu, J. Yan, W. Wu, F. Bai, and F. Huang, “Blast performance of 3D-printed auxetic honeycomb sandwich beams,” *Thin-Walled Structures*, 2023, [Online]. Available: https://api.semanticscholar.org/CorpusID:264053198
15. J. Yan *et al.*, “Ballistic characteristics of 3D-printed auxetic honeycomb sandwich panel using CFRP face sheet,” *International Journal of Impact Engineering*, 2022, [Online]. Available: https://api.semanticscholar.org/CorpusID:246422785
16. N. D. Dat, T. Q. Quan, and N. D. Duc, “Vibration analysis of auxetic laminated plate with magneto-electro-elastic face sheets subjected to blast loading,” *Composite Structures*, 2021, [Online]. Available: https://api.semanticscholar.org/CorpusID:243842344
17. Y. Wang, “Auxetic Composite Laminates with Through-Thickness Negative Poisson’s Ratio for Mitigating Low Velocity Impact Damage: A Numerical Study,” *Materials*, vol. 15, no. 19, Oct. 2022, doi: 10.3390/ma15196963.
18. R. Wang *et al.*, “Experimental Investigations on the Mechanical Performances of Auxetic Metal-Ceramic Hybrid Lattice under Quasi-Static Compression and Dynamic Ballistic Loading,” *Applied Sciences (Switzerland)*, vol. 13, no. 13, Jul. 2023, doi: 10.3390/app13137564.
19. D. Pawlus, “Static Stability of Composite Annular Plates with Auxetic Properties,” *Materials*, vol. 15, no. 10, May 2022, doi: 10.3390/ma15103579.
20. Kim. E., Roh J.-H., and Lee. I., “Numerical Analysis of SMA Hybrid Composite Plate Subjected to Low-Velocity Impact,” *International Journal of Aeronautical and Space Sciences*, vol. 8, no. 2, pp. 76–81, 2007, doi: 10.5139/IJASS.2007.8.2.076.
21. N. Novak, M. Vesenjak, G. Kennedy, N. N. Thadhani, and Z. Ren, “Response of Chiral Auxetic Composite Sandwich Panel to Fragment Simulating Projectile Impact,” *physica status solidi (b)*, vol. 257, 2019, [Online]. Available: https://api.semanticscholar.org/CorpusID:197514604
22. P. Sengsri and S. Kaewunruen, “Local failure modes and critical buckling loads of a meta-functional auxetic sandwich core for composite bridge bearing applications,” *Applied Sciences (Switzerland)*, vol. 11, no. 22, Nov. 2021, doi: 10.3390/app112210844.